Chapter 17

Structural Properties of Self-Assembled Monolayers on Gold Generated from Terminally Fluorinated Alkanethiols

Ramon Colorado, Jr., Michael Graupe, Olga E. Shmakova, Ramon J. Villazana, and T. Randall Lee*

Department of Chemistry, University of Houston, Houston, TX 77204–5641

This research examines the structural effects that accompany systematic alterations in the chemical composition of SAMs on gold prepared from three distinct series of terminally fluorinated alkanethiols having the general formula $F(CF_2)_x(CH_2)_ySH$. In the first series, the length of the fluorocarbon segment is varied (x = 1-10) while the length of the hydrocarbon segment is held constant (y = 11). In the second series, the length of the fluorinated segment is held constant (x = 10) while the length of the hydrocarbon segment is varied (y = 2-6, 11, and 17). In the final series, both the length of the fluorinated segment (x = 1-10) and the length of the hydrocarbon segment (y = 15-6, respectively) of hexadecanethiols are varied. Analyses of the films by ellipsometry and X-ray photoelectron spectroscopy (XPS) reflect the controlled introduction of fluorine within a series. Characterization of the monolayers by polarization modulation infrared reflection absorption spectroscopy (PM-IRRAS) reveals that the conformational order of the hydrocarbon segments in terminally fluorinated films varies systematically with the number of methylene units present, but is unaffected by the length of the overlying perfluorinated terminal segment.

Introduction

Fluorinated organic materials serve as useful coatings in a variety of applications involving computer hard disks, micro-electro-mechanical systems (MEMS), biomaterials, and non-stick coatings [1-4]. The physical properties of these materials (e.g., adhesion, friction, wettability, and thermal stability) are influenced by the

structure and composition of the surfaces [5-8]. To better understand this relationship, we evaluated the structural properties of a series of self-assembled monolayers (SAMs) on gold generated from alkanethiols that possess a systematically varied degree of terminal fluorination [9]. The following factors illustrate why the alkanethiolate SAM system is particularly well-suited for studying fluorinated organic interfaces: (1) the films are easy to make, (2) they are densely packed and highly oriented, and (3) their structure and composition can be altered through the use of standard organic synthetic methods [10]. We prepared SAMs on Au(111) from three distinct series of terminally fluorinated alkanethiols having the general formula $F(CF_2)_x(CH_2)_ySH$, in which the length of the fluorocarbon segment (x) and the length of the hydrocarbon segment (y) are varied (Figure 1). In Series 1, we maintain the length of the hydrocarbon segment while increasing the length of the fluorocarbon segment in adsorbates having the formula $F(CF_2)_x(CH_2)_{11}SH$, where x = 1-10. In Series 2, we increase the length of the hydrocarbon spacer while holding the length of the fluorocarbon segment constant in adsorbates having the formula $F(CF_2)_{10}(CH_2)_ySH$, where y = 2-6, and 11. In Series 3, we vary both the length of the hydrocarbon and fluorocarbon segments while holding the total chain length constant at 16 carbon atoms in adsorbates having the formula $F(CF_2)_x(CH_2)_ySH$, where x = 1-10 and y = 16-x, respectively. We characterized the films by ellipsometry, X-ray photoelectron spectroscopy (XPS), and polarization modulation infrared reflection absorption spectroscopy (PM-IRRAS).

Experimental

Ellipsometric Thicknesses. The thicknesses of the monolayers were measured with a Rudolph Research Auto EL III ellipsometer equipped with a He-Ne laser (632.8 nm) at an incident angle of 70° from the surface normal. A refractive index of 1.45 was assumed for all films. For a given sample, the data were averaged over three separate slides using three spots per slide.

Infrared Spectroscopy. Polarization modulation infrared reflection absorption spectroscopy (PM-IRRAS) data were collected using a Nicolet MAGNA-IR 860 Fourier transform spectrometer equipped with a liquid nitrogen-cooled mercury-cadmium-telluride (MCT) detector and a Hinds Instruments PEM-90 photoelastic modulator. The p-polarized light was incident at 80° from the surface normal. The spectra were collected for 1000 scans at a spectral resolution of 4 cm^{-1}.

X-ray Photoelectron Spectroscopy (XPS). A PHI 5700 X-ray photoelectron spectrometer equipped with an monochromatic Al Kα X-ray source (hν = 1486.7 eV) incident at 90° relative to axis of a hemispherical energy analyzer was used to obtain X-ray photoelectron spectra of freshly prepared samples. The spectrometer was configured to operate at high resolution with a pass energy of 23.5 eV, a photoelectron takeoff angle of 45° from the surface, and an analyzer spot diameter of 1.1 mm. Spectra were collected at room temperature and a base pressure of 2×10^{-9} torr for the following elements: C 1s (8 scans over 1.67 min) and Au 4f (4 scans over 0.67 min). Standard curve-fitting software using Shirley background subtraction and

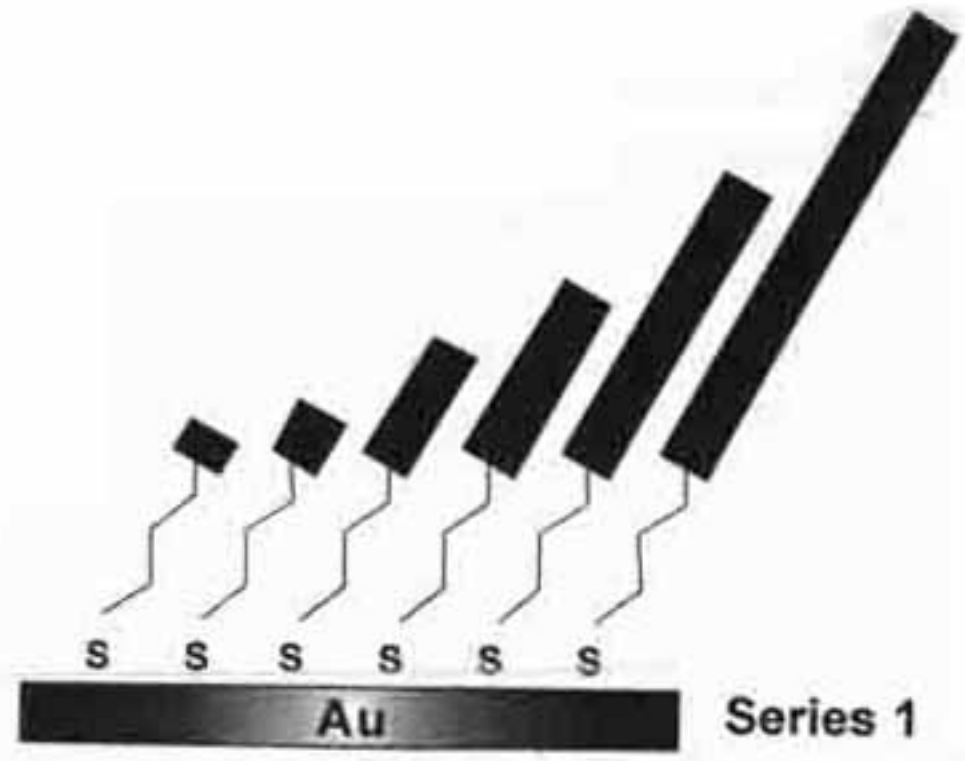

Figure 1. Illustration of SAMs on gold derived from the adsorption three distinct series of terminally fluorinated alkanethiols.

Gaussian-Lorentzian profiles was used to determine the peak intensities. All peaks were fit with respect to spin-orbit splitting. A 100% Gaussian curve was used for the C 1s peaks. Two 65% Gaussian curves in a 3:4 area ratio split by 3.67 eV were used for the Au 4f peaks. The constancy of the F 1s peak intensities for the films indicated that little or no damage occurred to the film during the data acquisition.

Results and Discussion

Ellipsometry

Ellipsometry is commonly used to evaluate the thickness of organic thin films [10]. While considerable experimental uncertainties might often accompany ellipsometric measurements (e.g., ± 2 Å), the technique is, nevertheless, useful for evaluating changes in film thickness within a series of films in which the structure changes subtly and systematically [11,12]. Figure 2a shows the thicknesses obtained for films from Series 1. The thicknesses increase linearly with an increase in the number of fluorinated carbon atoms (*ca.* 1.23 Å per CF_2 unit) [13]. Errors, however, associated with measurements of ellipsometric thickness preclude a rigorous evaluation of the chain tilt and/or twist in these films. These measurements merely reflect the expected increase in film thickness that accompanies the adsorption of progressively longer molecules.

Figure 2b shows the ellipsometric thicknesses of SAMs from Series 2. In this series, the thicknesses of the films generated from $F(CF_2)_{10}(CH_2)_ySH$ with y = 2-6, 11, and 17 increase linearly as the number of CH_2 groups increases (*ca.* 1.18 Å per CH_2), again reflecting the increase in thickness that accompanies the adsorption of progressively longer molecules [13].

Figure 2c plots the thicknesses of SAMs from Series 3 versus the number of fluorinated carbon atoms. For the entire series, the thickness remains relatively constant (~ 16 Å). Therefore, the results appear to reflect the constant total chain length of the adsorbates. We have recently reported that, within a SAM, the tilt angle with respect to the surface normal of the fluorocarbon segment of constant length increases as the length of the hydrocarbon segment increases [14,15]. Since the changing tilt of the fluorinated segment with the decreasing length of the hydrocarbon segment within SAMs from Series 3 might be expected to influence film thickness, the results also demonstrate that ellipsometry is insensitive to any of these potential changes in thickness.

X-ray Photoelectron Spectroscopy

XPS Intensity of the Au 4f Photoelectrons. The attenuation of gold photoelectrons emitted from a SAM is related to the thickness of the organic overlayer [16,17]. This relationship offers an opportunity to monitor the changes in the monolayer thickness that accompany chemical and structural changes of the adsorbates. Figure 3a shows the natural logarithm of the Au 4f photoelectron intensity as a function of the number

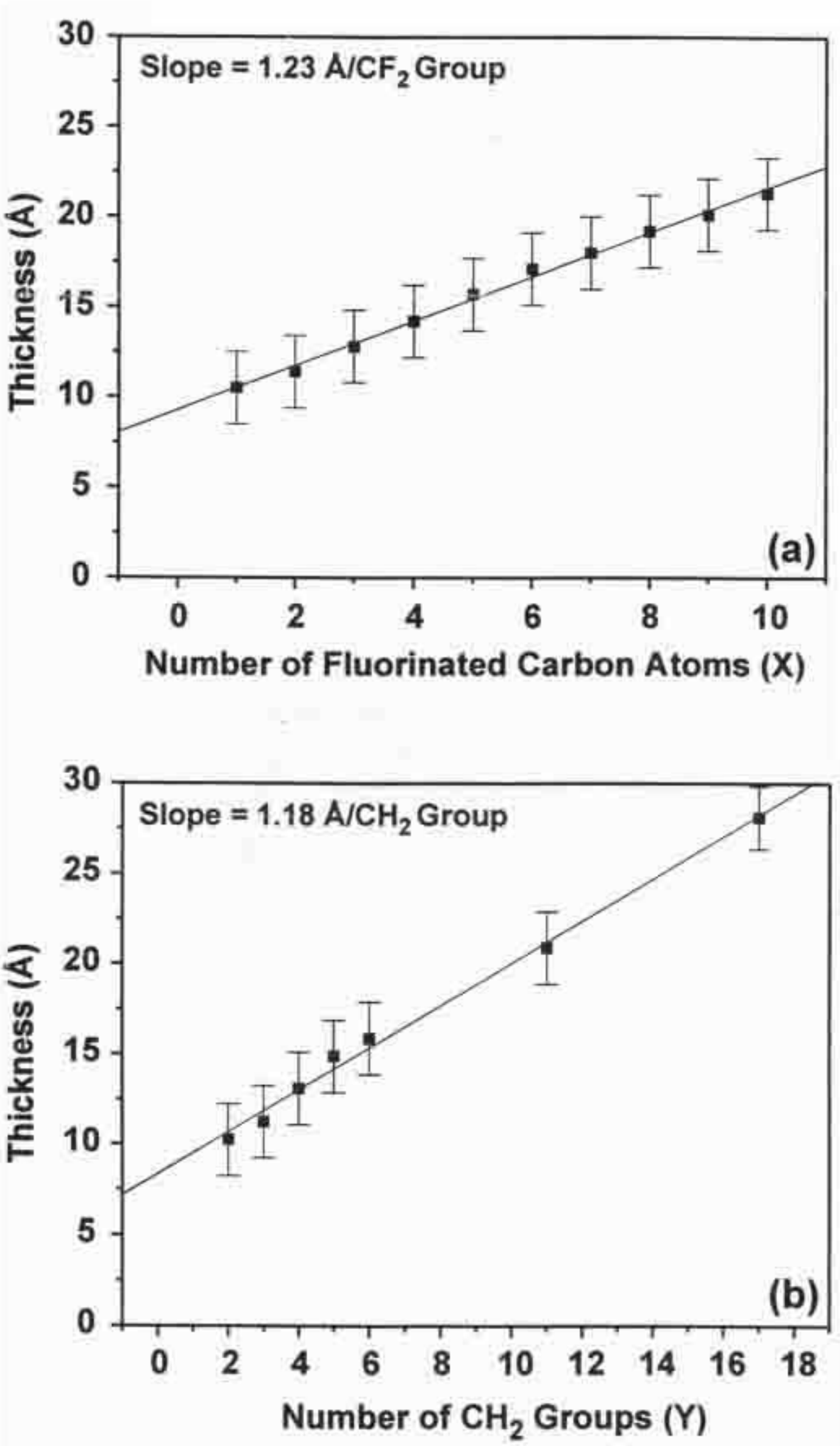

Figure 2. Average ellipsometric thickness of (a) SAMs from Series 1, (b) SAMs from Series 2, and (c) SAMs from Series 3. All measured thicknesses were reproducible within ± 2 Å of the reported average value.

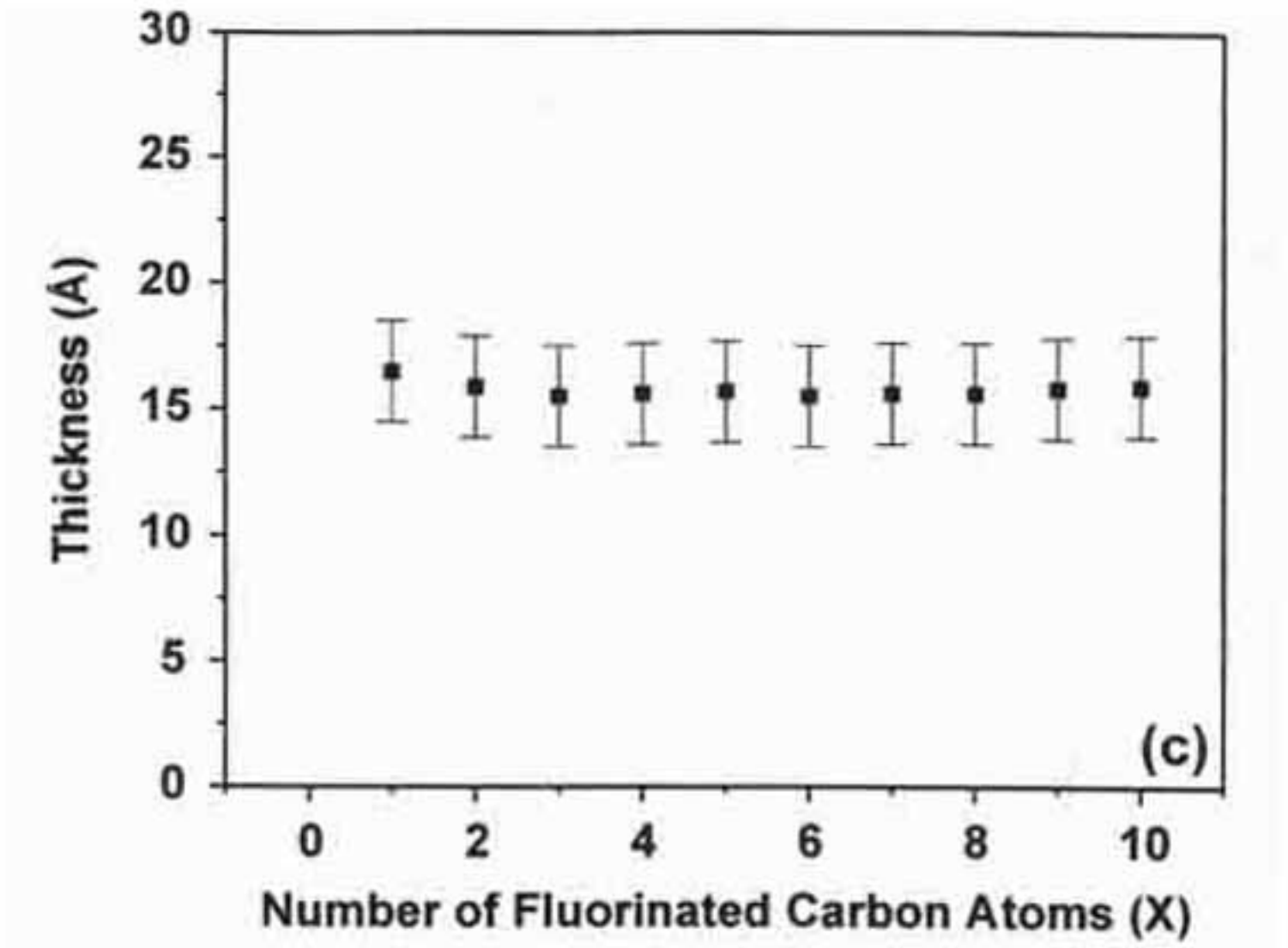

Figure 2. Continued.

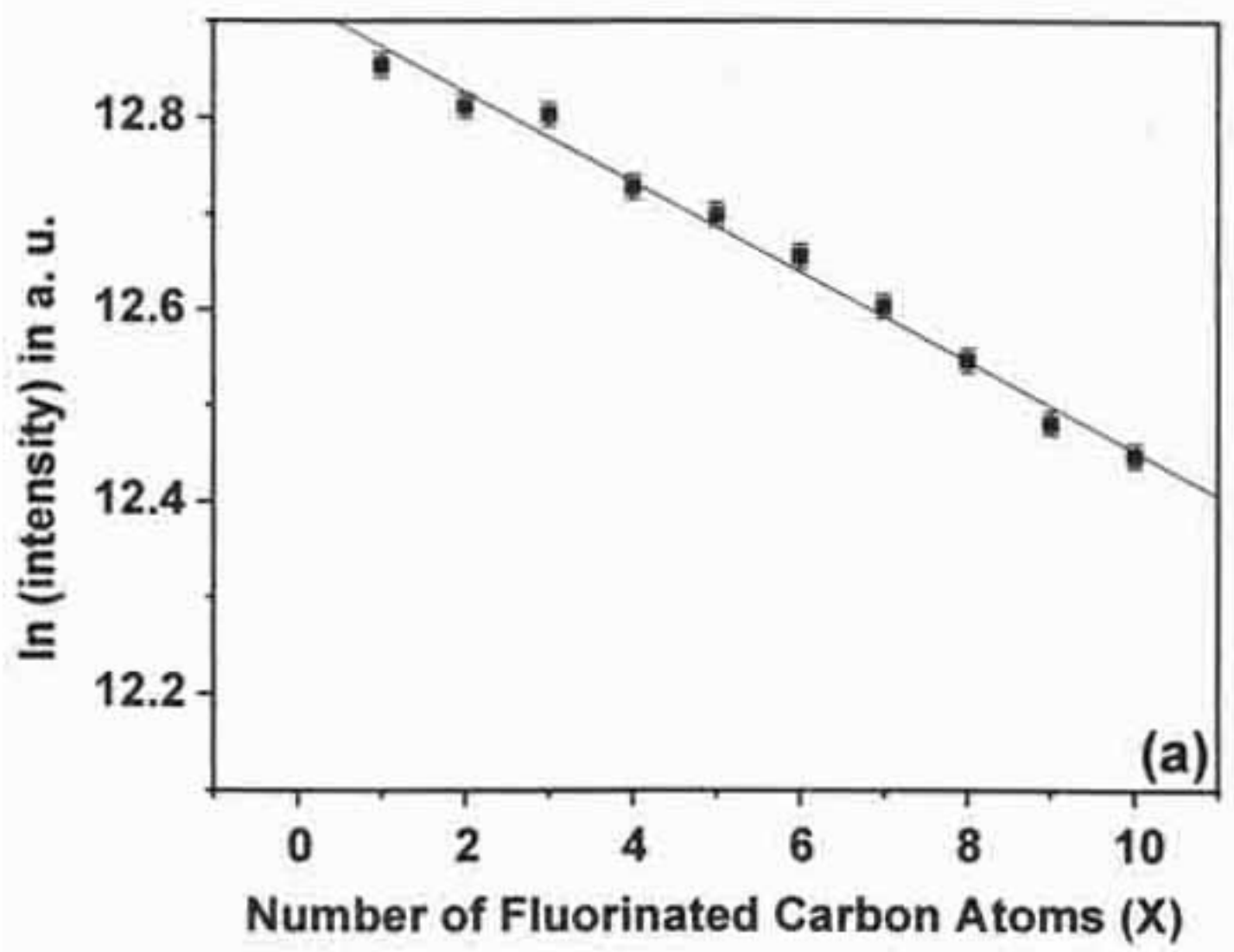

Figure 3. Intensity of Au 4f photoelectrons emitted from (a) SAMs from Series 1, (b) SAMs from Series 2, and (c) SAMs from Series 3. All measured intensities were reproducible within ± 1% of the reported average value, as determined by the standard deviation of four measurements per sample. The lines through the data are intended solely to guide the eye.

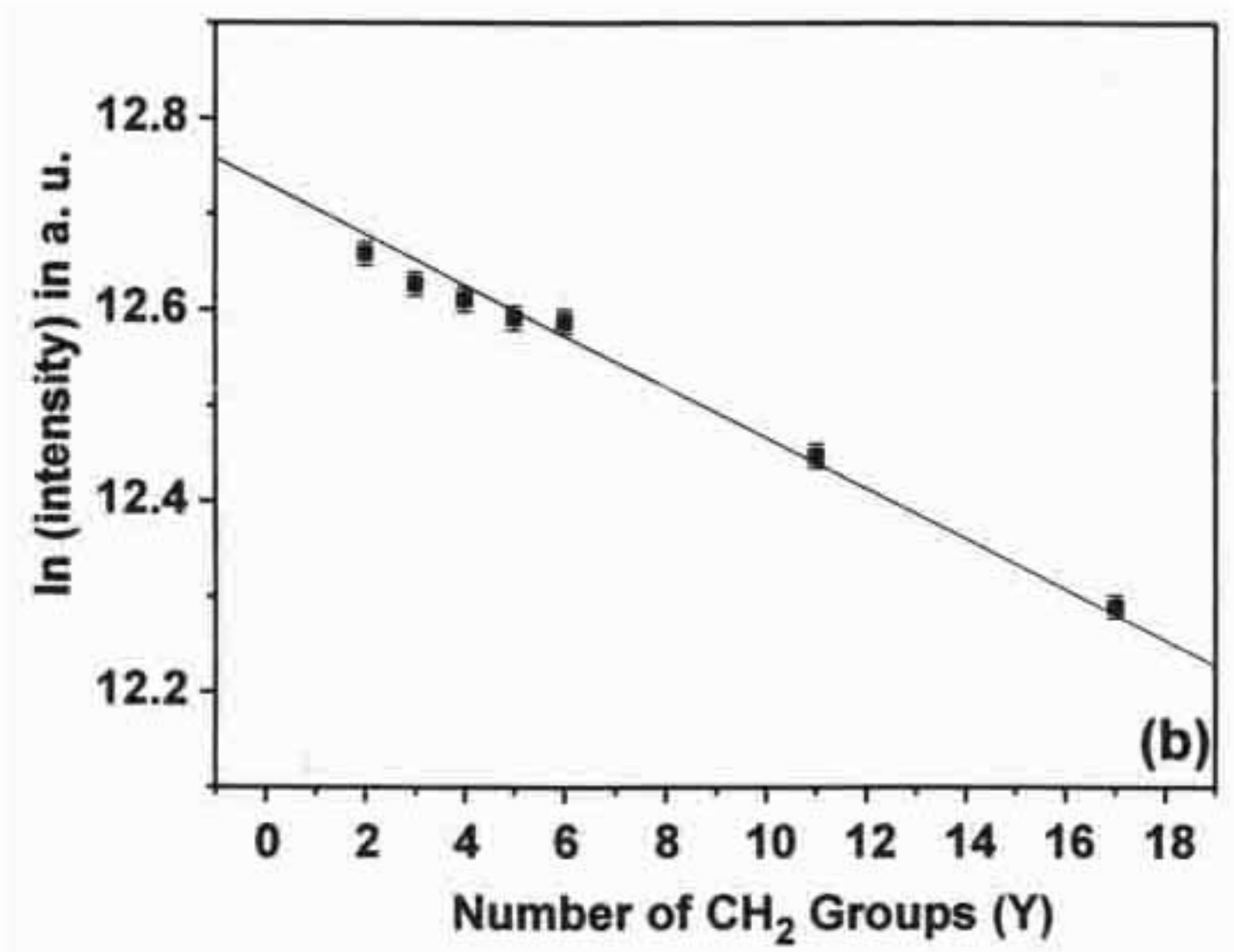

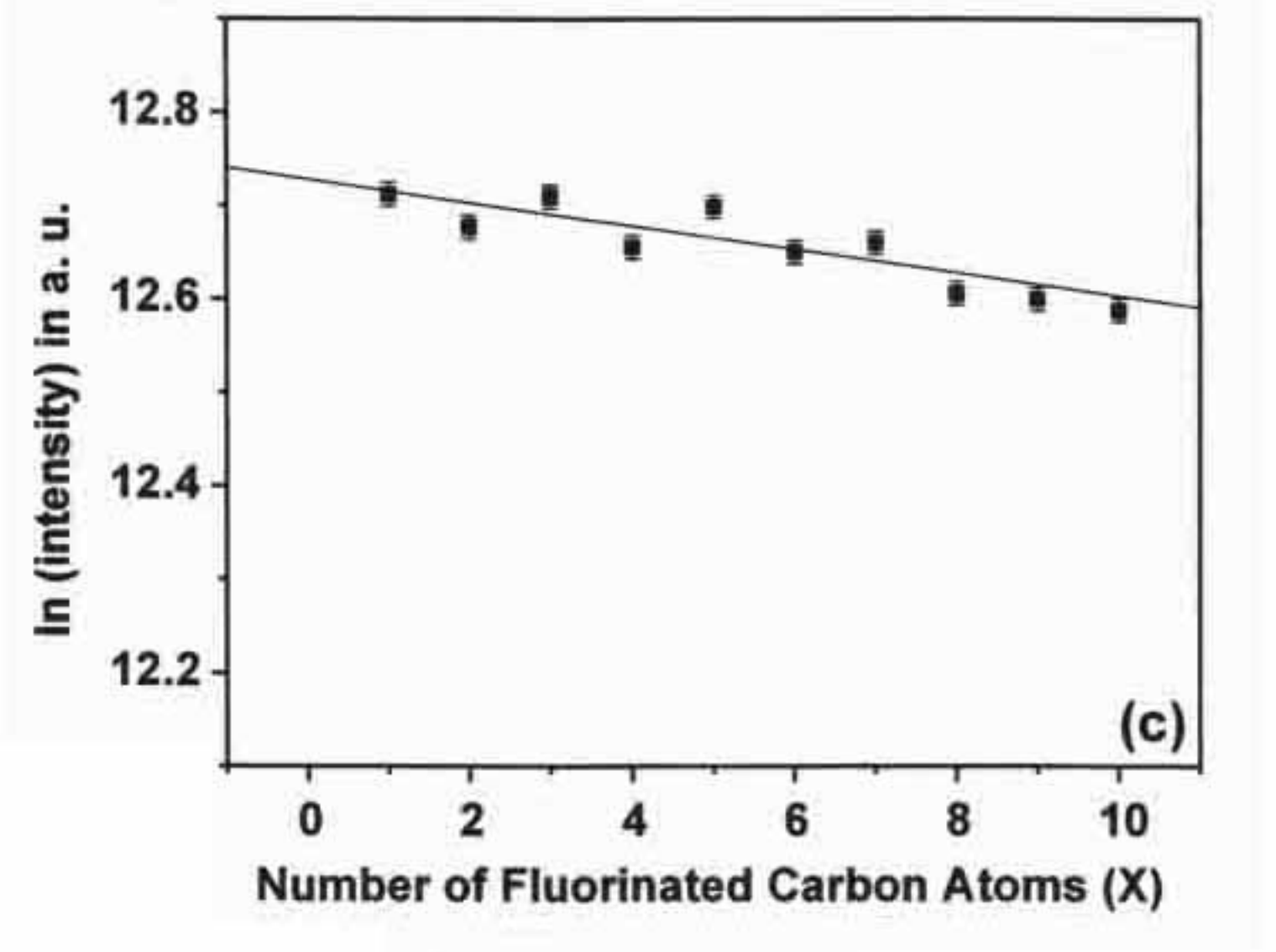

Figure 3. Continued.

of fluorinated carbon atoms in SAMs from Series 1. The natural logarithms of the intensities decrease linearly as the length of the fluorinated segment increases. This trend reflects an increased attenuation of the gold signal as the overall thickness of the monolayers increase. Although similar plots can be used to determine absolute thicknesses in hydrocarbon SAM systems [18], we are unable to calculate the absolute thicknesses of our terminally fluorinated SAMs because both the attenuation length of photoelectrons through fluorocarbons and the twists and tilts of the hydrocarbon and fluorocarbon segments within each film are presently unknown.

Figure 3b shows the attenuation of the gold photoelectrons as a function of the number of CH_2 groups in SAMs from Series 2. The films generated from these adsorbates exhibit a linear decrease in the natural logarithm of intensity as the length of the hydrocarbon segments increase.

Figure 3c plots the natural logarithm of the photoelectron intensity for SAMs from Series 3 versus the number of fluorinated carbons. Like the ellipsometric data for these SAMs, the values remain within a narrow range. The natural logarithm of the intensities, however, appears to decrease as the degree of fluorination increases. If we assume a constant thickness for the SAMs in this series, this trend appears consistent with an enhanced attenuation of Au 4f photoelectrons by CF_2 groups relative to that of CH_2 groups that occurs as the number of fluorinated carbon atoms increases at the expense of the number of CH_2 groups. Changes in the tilt of the fluorocarbon or hydrocarbon segments, however, might also influence the thickness of the films and give rise to the observed trends in attenuation.

XPS Intensity of the C 1s Photoelectrons. The carbon 1s photoelectron spectrum can be used to monitor the relative amounts of fluorocarbon and hydrocarbon in thin films [8]. The peaks arising from CH_2 and CF_2 segments have the following distinct binding energies: 285 eV and 290 eV, respectively. Figure 4a shows the XPS intensities of both the CH_2 and CF_2 C 1s photoelectrons versus the number of fluorinated carbon atoms in SAMs from Series 1. The CF_2 photoelectrons exhibit an expected exponential increase in intensity as the length of the fluorinated segment increases. Although the CH_2 signal for every film in Series 1 arises from an equivalent number of methylene units, the CH_2 photoelectron intensities also exhibit a dependence on the length of the fluorocarbon segment. The intensities of these peaks decrease as the fluorocarbon segment increases in length because the photoelectrons are attenuated more as the number of overlying CF_2 groups increases.

The XPS intensity of the C 1s photoelectrons as a function of the number of CH_2 groups in SAMs from Series 2 is shown in Figure 4b. The CF_2 intensities reflect the constant length of the fluorocarbon segment and remain constant as the length of the hydrocarbon segment increases. As expected, the CH_2 intensities increase exponentially as the length of the hydrocarbon segment increases.

Figure 4c shows the C 1s photoelectron intensities versus the number of fluorinated carbon atoms in SAMs from Series 3. The increase of the CF_2 intensities with increasing length of the fluorocarbon segment is similar to the increase seen for the films from Series 1. In contrast, the CH_2 intensities in the SAMs from Series 3 decrease more than in the films from Series 1 with increasing length of the

fluorocarbon segment. These results suggest that in addition to the increased attenuation by the overlying fluorocarbon segment (which is equivalent in both series), the decreasing number of CH_2 groups in SAMs from Series 3 in comparison to the constant number of CH_2 groups in SAMs from Series 1 serves to lower the methylene photoelectron signal in Series 3.

Polarization Modulation Infrared Reflection Absorption Spectroscopy

Axial Fluorocarbon Band Positions. We obtained spectra of the C-F stretching regions of the SAMs using PM-IRRAS. Two bands that are of particular interest in characterizing the fluorocarbon segments of semifluorinated films are the first and second axial vibrations that occur at 1315-1345 cm^{-1} and 1365-1375 cm^{-1}, respectively [14,19-22]. These bands arise from the helical conformation of the fluorocarbon segment; moreover, the band positions depend on the size of the fluorocarbon helix [20,22]. Figure 5a shows the positions of the axial bands as a function of the number of fluorinated carbon atoms in SAMs from Series 1. As the length of the fluorinated segment increases, both band positions move progressively toward higher wavenumbers. Figure 5b shows the axial band positions versus the number of CH_2 groups in SAMs from Series 2. Since the length of the fluorinated segment remains constant in this series, both band positions remain constant. Figure 5c shows the positions of the axial bands as a function of the number of fluorinated carbon atoms in SAMs from Series 3. Not only do the band positions of these films increase with the length of the fluorocarbon segment as in the films from Series 1, the band positions from a given fluorocarbon length are identical to those in films from Series 1. Since the tilts for fluorocarbon segments of equivalent length in both series are likely to be different [14,15], these results suggest that the absolute position of the axial bands can be used to determine the length of fluorocarbon segments in SAMs without regard to the orientation of the segments within the film.

Antisymmetric CH_2 Band Positions. The position of the antisymmetric methylene band in normal alkanethiol SAMs is sensitive to the conformational order of the hydrocarbon chains [10,23-25]. Shifts of these bands to higher wavenumbers are associated with decreases in interchain van der Waals interactions and increases in intrachain gauche defects (i.e., more liquid-like conformational states) [10,23-25]. Figure 6 shows the antisymmetric methylene band position as a function of the total number of carbon atoms in SAMs derived from a series of normal alkanethiols. The results are consistent with a model in which the conformational order (or crystallinity) of the films increases with increasing chain length [10,23].

We examined the antisymmetric methylene band position versus the number of fluorinated carbon atoms in SAMs from Series 1. Figure 7a shows that the band position remains constant as the length of the fluorinated segment increases. These data suggest that the introduction of longer fluorinated segments into the upper portion of the films induces no conformational disordering of the underlying hydrocarbon segments.

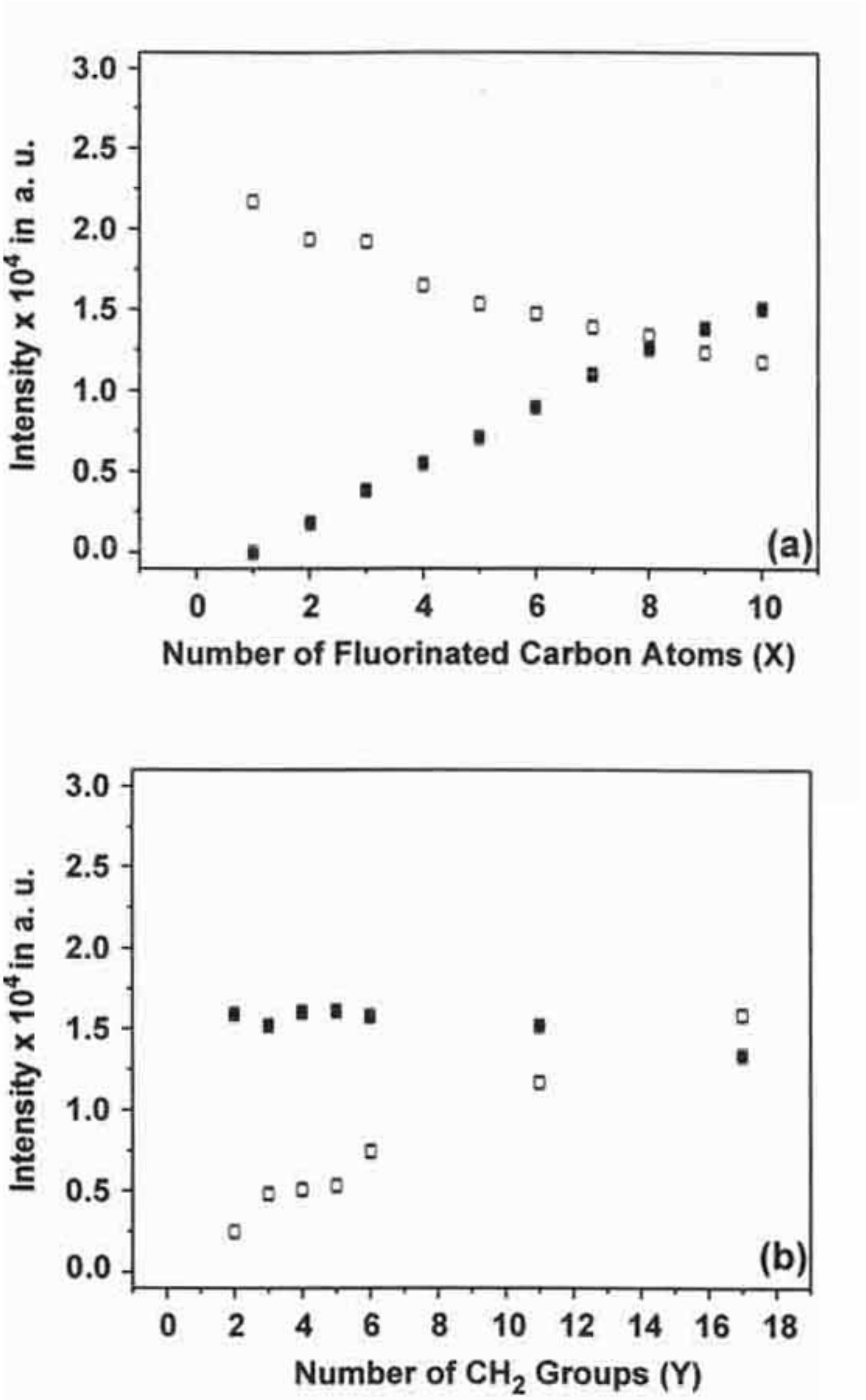

Figure 4. Intensity of fluorocarbon (open squares) and hydrocarbon (filled squares) C 1s photoelectrons emitted from (a) SAMs from Series 1, (b) SAMs from Series 2, and (c) SAMs from Series 3. All measured intensities were reproducible within ± 2% of the reported average value, as determined by the standard deviation of four measurements per sample.

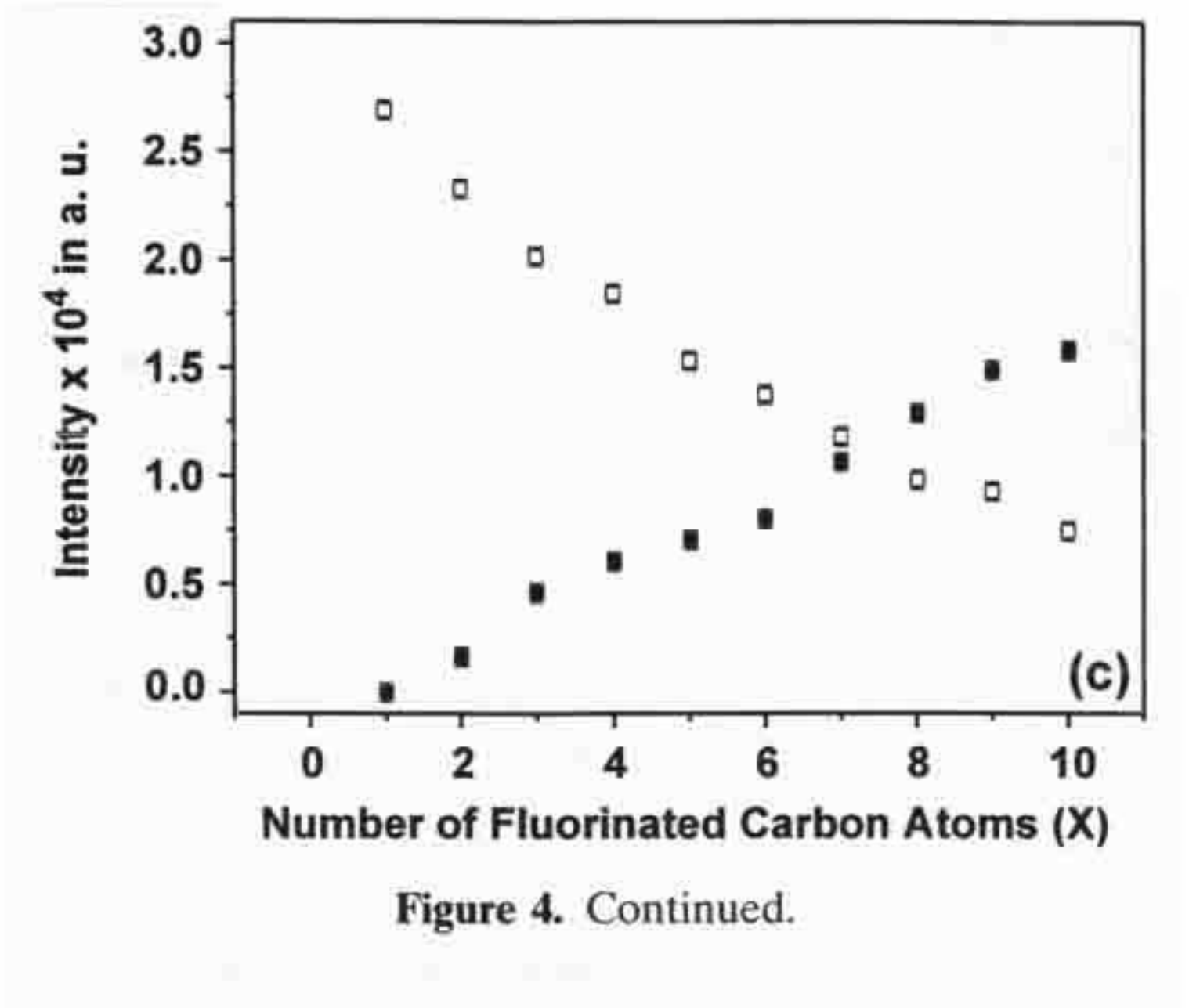

Figure 4. Continued.

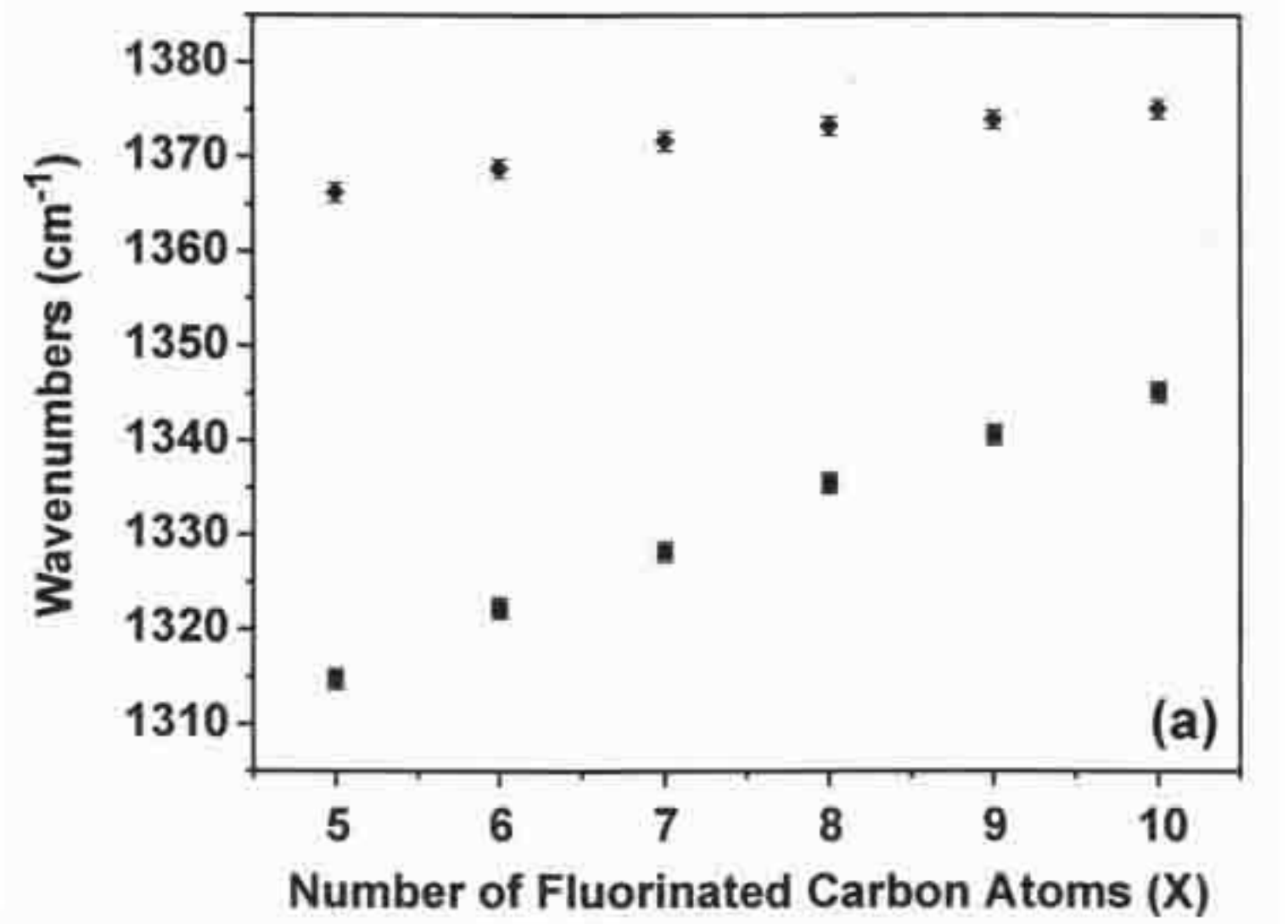

Figure 5. Average band positions of the first (■) and second (◆) axial vibrations of fluorocarbon segments in (a) SAMs from Series 1, (b) SAMs from Series 2, and (c) SAMs from Series 3. All measured band positions were reproducible within ± 0.5 cm^{-1} of the reported average value.

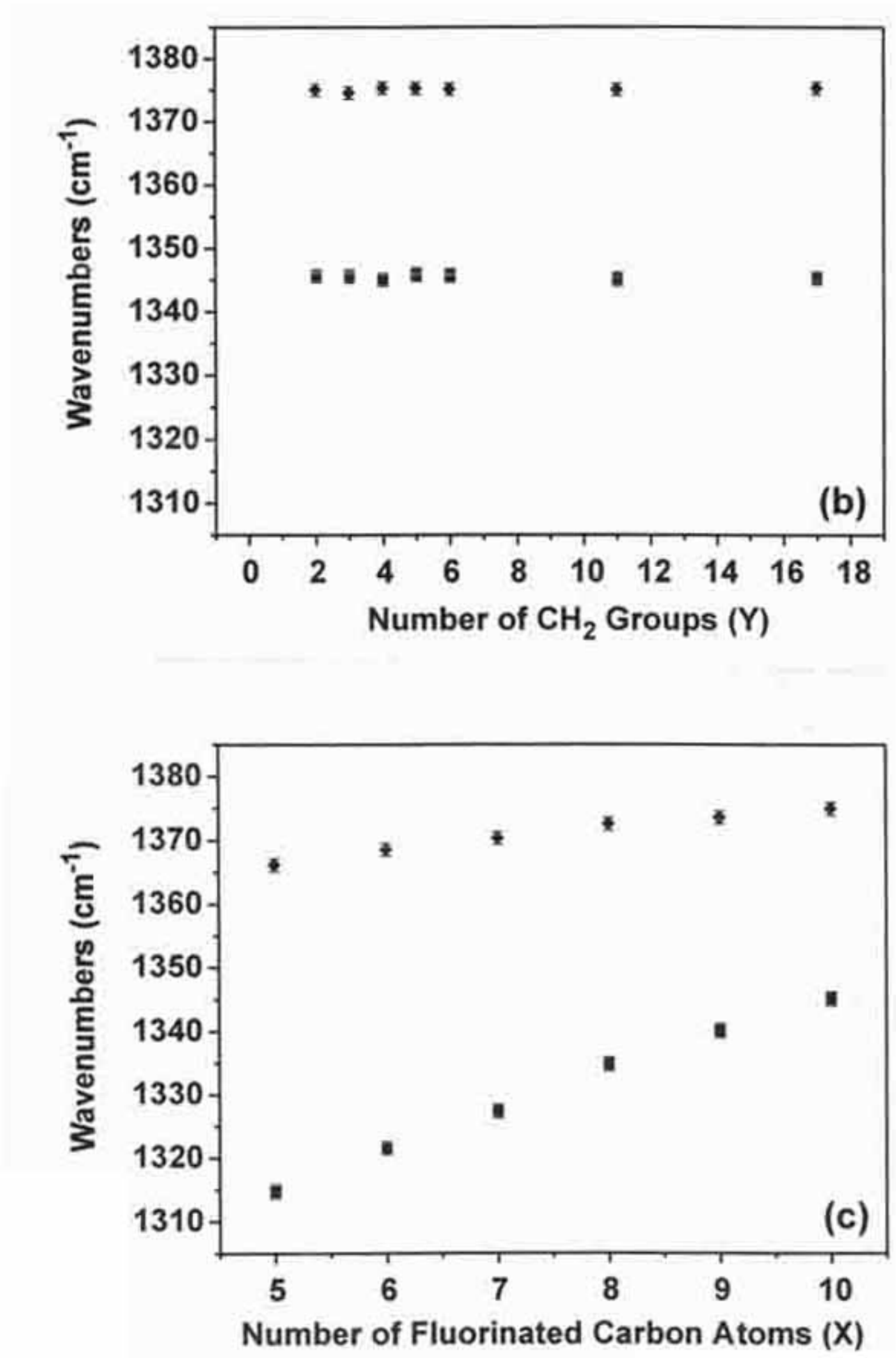

Figure 5. Continued.

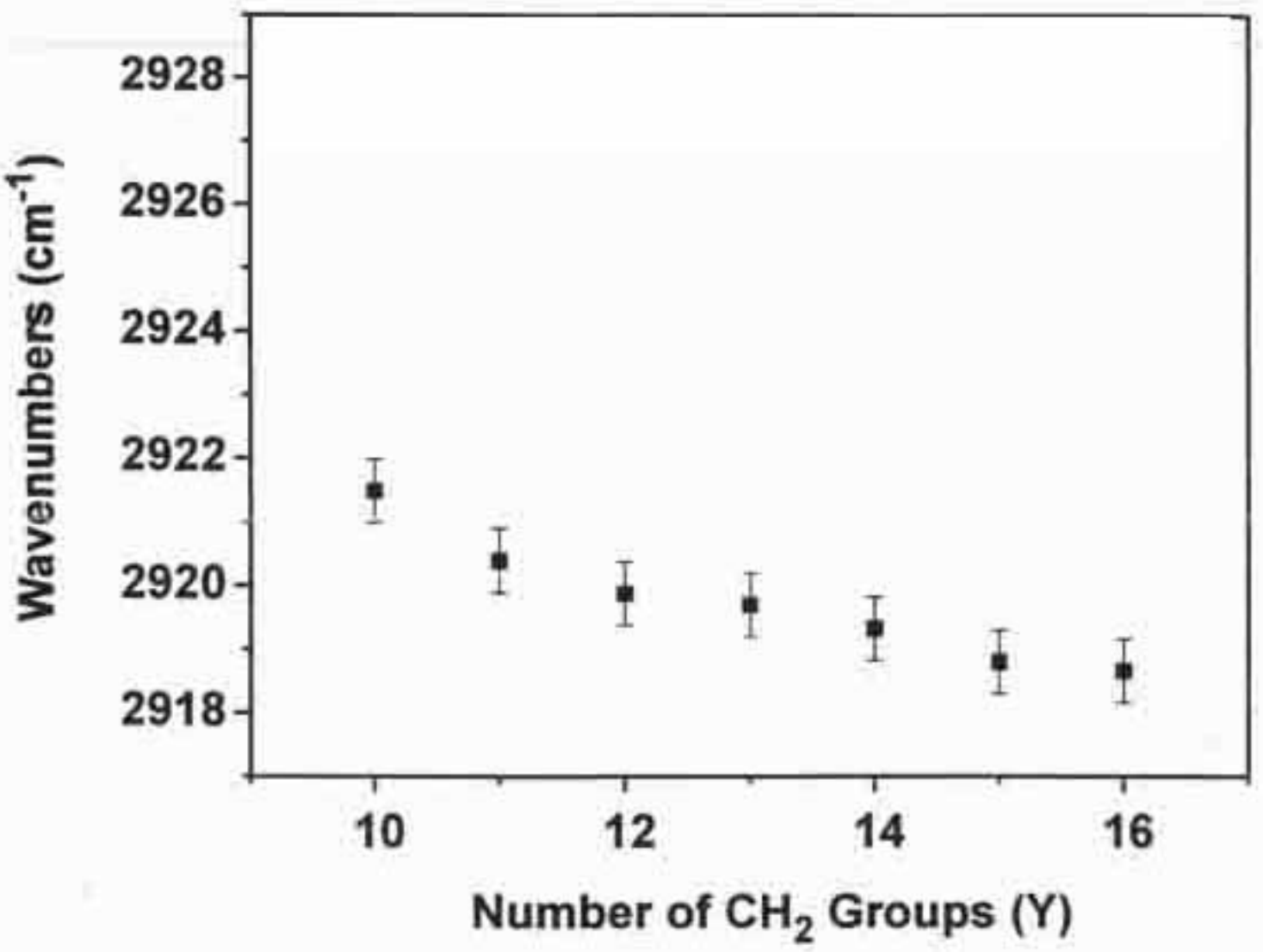

Figure 6. Average antisymmetric methylene band position ($\nu_a^{CH_2}$) of the hydrocarbon backbone in SAMs from normal alkanethiols. All measured band positions were reproducible within ± 0.5 cm^{-1} of the reported average value.

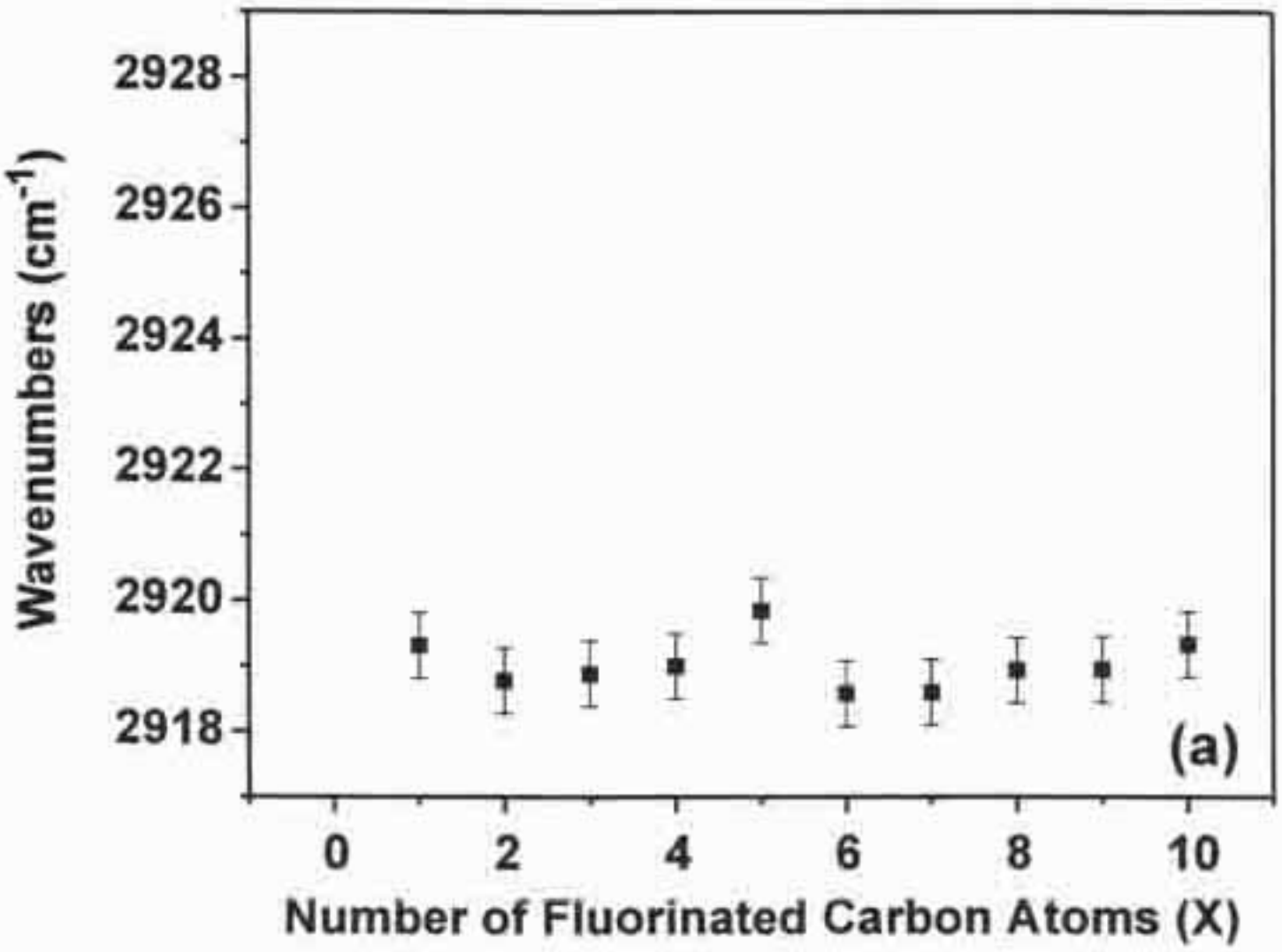

Figure 7. Average antisymmetric methylene band position ($\nu_a^{CH_2}$) of the hydrocarbon segments in (a) SAMs from Series 1, (b) SAMs from Series 2, and (c) SAMs from Series 3. All measured band positions were reproducible within ± 0.5 cm^{-1} of the reported average value.

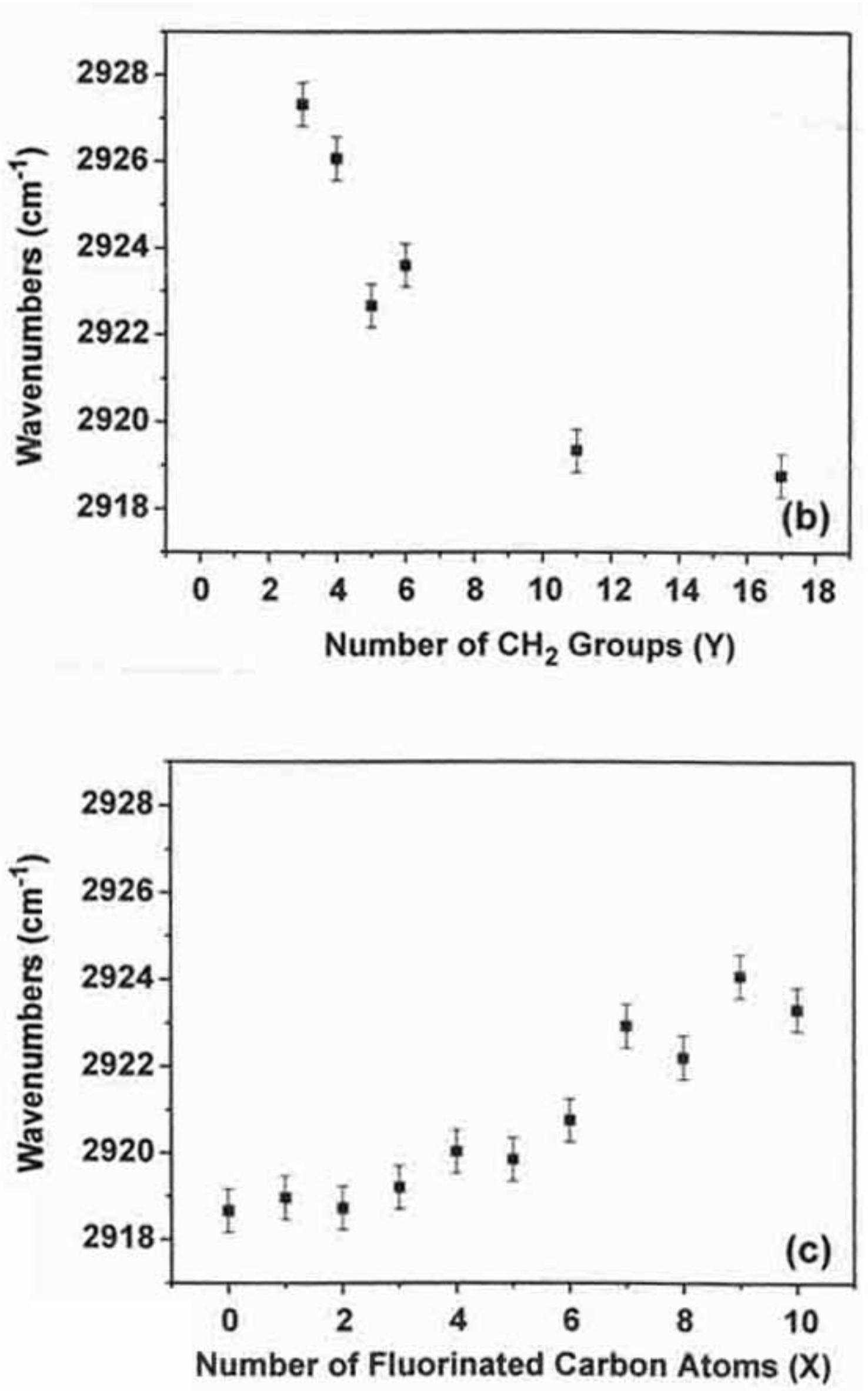

Figure 7. Continued.

Figure 7b shows the antisymmetric methylene band position as a function of the number of CH_2 groups in SAMs from Series 2. As the length of the hydrocarbon segment increases, the band position shifts to lower wavenumber. Consequently, it appears that in films with overlying fluorinated helices of constant size, increasing the number of methylene units leads to more conformationally ordered hydrocarbon underlayers.

Figure 7c plots the antisymmetric methylene band position versus the number of fluorinated carbon atoms in SAMs from Series 3. As the length of the fluorinated segment increases, the band position shifts to higher wavenumber, indicating a decrease in the conformational order of the hydrocarbon backbone [23-25]. Given the aforementioned results for the other two fluorinated series, we believe that the decrease in conformational order arises primarily from decreasing the length of the hydrocarbon segment (loss of strong van der Waals interactions), which reduces the number of stabilizing interchain van der Waals interactions, and is largely unaffected by increasing the length of the fluorinated segment (gain of weaker van der Waals interactions).

Conclusions

We have prepared and characterized SAMs from three distinct series of terminally fluorinated alkanethiols to probe the relationships between the introduction of fluorine and the structure of fluorinated organic thin films. The trends in ellipsometric thickness are consistent with the expected changes in adsorbate length. Characterization of the films by XPS demonstrates that the attenuation of Au 4f photoelectrons follows the expected logarithmic dependence on the total chain length of the adsorbates. Since, however, the attenuation length of photoelectrons through fluorocarbons and the twist and/or tilt angles of the fluorocarbon and hydrocarbon segments in the films are unknown, we are currently unable to calculate absolute film thicknesses from the Au 4f XPS data. Furthermore, as fluorine is systematically introduced into the monolayers, the intensity of the fluorinated C 1s photoelectrons increase exponentially at the expense of the hydrocarbon C 1s photoelectrons. PM-IRRAS studies of the SAMs from Series 1 suggest that the hydrocarbon segments of constant chain length remain ordered upon increasing the length of the fluorinated segment. In SAMs from Series 2 with a constant length of the fluorinated segment, the hydrocarbon segments become more ordered with increasing chain length. In SAMs from Series 3, the hydrocarbon segments become more disordered with decreasing length. This trend appears to arise predominately from the net loss of van der Waals stabilization that accompanies the substitution of CF_2 for CH_2. Taken together, these data suggest that systematic alterations of the adsorbates used to generate SAMs can effect systematic structural changes in the resultant films. Further investigations of the structure of these monolayers by atomic force microscopy (AFM) and near-edge X-ray absorption fine structure spectroscopy (NEXAFS) are ongoing. We are also exploring the influence of these structural changes upon the thermal stabilities of the films.

Acknowledgements

We thank the National Science Foundation (DMR-9700662) and Seiko Epson Corporation for financial support. We also thank Professor Jan Genzer (North Carolina State University) and Dr. Hitoshi Fukushima (Seiko Epson) for helpful discussions. R.C. acknowledges the NRC-Ford Foundation and the UH Center for Mexican-American Studies for predoctoral fellowships. This work made use of MRSEC/TCSUH Shared Experimental Facilities supported by the National Science Foundation under Award Number DMR-9632667 and the Texas Center for Superconductivity at the University of Houston.

References

1. Homola, A. M.; Mate, C. M.; Street, G. B. *MRS Bull.* **1990**, *15*, 45.
2. Deng, K.; Collins, R. J.; Mehregany, M.; Sukenik, C. N. *J. Electrochem. Soc.* **1995**, *142*, 1278.
3. Ishihara, K. *Biomedical Applications of Polymeric Materials*, CRC Press: Boca Raton, 1993.
4. Kinloch, A. J. *Adhesion and Adhesives*, Chapman and Hall: New York, 1987.
5. Kim, H. I.; Koini, T.; Lee, T. R.; Perry, S. S. *Langmuir* **1997**, *13*, 7192.
6. Kim, H. I.; Graupe, M.; Oloba, O.; Koini, T.; Imaduddin, S.; Lee, T. R.; Perry, S. S. *Langmuir* **1999**, *15*, 3179.
7. Graupe, M.; Takenaga, M.; Koini, T.; Colorado, R., Jr.; Lee, T. R. *J. Am. Chem. Soc.* **1999**, *121*, 3222.
8. Schonherr, H.; Ringsdorf, H.; Jaschke, M.; Butt, H.-J.; Bamberg, E.; Allinson, H.; Evans, S. D. *Langmuir* **1996**, *12*, 3898.
9. Graupe, M.; Koini, T.; Wang, V. Y.; Nassif, G. M.; Colorado, R., Jr.; Villazana, R. J.; Dong, H.; Miura, Y. F.; Shmakova, O. E.; Lee, T. R. *J. Fluorine Chem.* **1993**, *93*, 107.
10. Ulman, A. *An Introduction to Ultrathin Organic Films*, Academic: Boston, 1991.
11. Bain, C. D.; Troughton, E. B.; Tao, Y.-T.; Evall, J.; Whitesides, G. M.; Nuzzo, R. G. *J. Am. Chem. Soc.* **1989**, *111*, 321.
12. Gupta, V. K.; Abbott, N. L. *Langmuir* **1996**, *12*, 2587.
13. The incremental increases in thickness for Figures 2a and 2b are the slopes of lines obtained by fitting the ellipsometric data for Series 1 and 2, respectively, by least-squares linear regression ($R^2 = 0.98$).
14. Tamada, K.; Nagasawa, J.; Nakanishi, F.; Abe, K.; Hara, M.; Knoll, W.; Ishida, T.; Fukushima, H.; Miyashita, S., Usui, T.; Koini, T.; Lee, T. R. *Thin Solid Films* **1998**, *327-329*, 150.

15. Fukushima, H.; Seki, S.; Nishikawa; Miyashita, S.; Tamada, K.; Nakanishi, F.; Abe, K.; Colorado, R., Jr.; Shmakova, O. E.; Graupe, M.; Lee, T. R., *J. Phys. Chem. B*, submitted.
16. Bain, C. D.; Whitesides, G. M. *J. Phys. Chem.* **1989**, *93*, 1670.
17. Laibinis, P. E.; Bain, C. D.; Whitesides, G. M. *J. Phys. Chem.* **1991**, *95*, 7017
18. Harder, P.; Grunze, M.; Dahint, R.; Whitesides, G. M.; Laibinis, P. E. *J. Phys. Chem. B* **1998**, *102*, 426.
19. Lenk, T. J.; Hallmark, V. M.; Hoffmann, C. L.; Rabolt, J. F.; Castner, D. G.; Erdelen, C.; Ringsdorf, H. *Langmuir* **1994**, *10*, 4610.
20. Tsao, M.-W.; Hoffmann, C. L.; Rabolt, J. F.; Johnson, H. E.; Castner, D. G.; Erdelen, C.; Ringsdorf, H. *Langmuir* **1997**, *13*, 4317.
21. Rabolt, J. F.; Russell, T. P.; Twieg, R. J. *Macromolecules* **1984**, *17*, 2786.
22. Naselli, C.; Swalen, J. D.; Rabolt, J. F. *J. Chem. Phys.* **1989**, *90*, 3855.
23. Porter, M. D.; Bright, T. B.; Allara, D. L.; Chidsey, C. E. D. *J. Am. Chem. Soc.*, **1987**, *109*, 3559.
24. Terrill, R. H.; Tanzer, T. A.; Bohn, P. W. *Langmuir* **1998**, *14*, 845.
25. Synder, R. G.; Strauss, H. L.; Elliger, C. A. *J. Phys. Chem.* **1982**, *86*, 5145.